

Effect of heating process on fracture behaviors of $W_f/Cu_{82}Al_{10}Fe_4Ni_4$ composites

Z. Wu · P. C. Kang · G. H. Wu · Q. Guo ·
Z. Y. Xiu

Received: 12 January 2011 / Accepted: 22 March 2011 / Published online: 1 April 2011
© Springer Science+Business Media, LLC 2011

Abstract $W_f/Cu_{82}Al_{10}Fe_4Ni_4(30)$ composites and $W_f/Cu_{82}Al_{10}Fe_4Ni_4(60)$ composites were prepared by penetrating casting method. Three-point bending test and dynamic compression test showed that $W_f/Cu_{82}Al_{10}Fe_4Ni_4(30)$ composites possessed higher mechanical properties than $W_f/Cu_{82}Al_{10}Fe_4Ni_4(60)$ composites. Microstructure observation of $W_f/Cu_{82}Al_{10}Fe_4Ni_4(30)$ composites revealed that a small amount of tungsten diffused into the Fe–Ni solid solution precipitated on the surface of tungsten fibers. The damage occurred mainly within the tungsten fibers after three-point bending test and dynamic compression test in $W_f/Cu_{82}Al_{10}Fe_4Ni_4(30)$ composites, indicating that the composites possessed high interface strength. Dislocation density was high and stacking faults emerged in $W_f/Cu_{82}Al_{10}Fe_4Ni_4(30)$ composites after dynamic compression. Microstructure observation of $W_f/Cu_{82}Al_{10}Fe_4Ni_4(60)$ composites revealed that long strip of tungsten grains occurred at the edge of tungsten fibers, within which damage mainly emerged after three-point bending test, indicating that strength of the edge of tungsten fibers was low in $W_f/Cu_{82}Al_{10}Fe_4Ni_4(60)$ composites. The fibrous structure of tungsten fiber was coarse or even disappeared in some areas, and dislocation density was low in $W_f/Cu_{82}Al_{10}Fe_4Ni_4(60)$ composites after dynamic compression.

Introduction

As the development of armor piercing bullet to high speed, high strength, and high density, the demand to mechanical property of the material used in armor piercer also increase [1–3]. Composites are composed of two or more kinds of materials reasonably, so they often possess better performance than single material. At present, many countries start to do research in composites' armor piercing bullet [4–6]. Tungsten fiber possesses high density, and it is drawn out from block tungsten under high-temperature [7–9]. During the drawing process, the inner structure of tungsten fiber will be fiberized, so the tungsten fiber possesses high mechanical property [10, 11]. Due to these advantages, tungsten fiber is selected as reinforcement of the composites in this paper. Because copper alloy possesses high density and high strength, and W–Cu composites have been successfully used in many fields including electronics, military, aerospace, copper alloy is selected as matrix, in which iron, nickel, and aluminum were added in order to improve interface strength of the composites [12–16]. Because high-temperature will crucially affect the final mechanical property and microstructure of tungsten fiber in the composites, we selected two kinds of heating processes to fabricate the composites in this paper. Then bending strength and dynamic mechanical property of the composites were tested, and microstructure and fracture mechanism of the composites were analyzed in order to find the better heating processes.

Materials and experimental methods

$Cu_{82}Al_{10}Fe_4Ni_4$ alloy was selected as the matrix in this paper. The diameter of tungsten fiber is 0.25 mm. After straightening, tungsten fibers were cut into 100 mm long and

Z. Wu (✉) · P. C. Kang · G. H. Wu · Q. Guo · Z. Y. Xiu
School of Materials Science and Engineering, Harbin Institute
of Technology, P. O. 3023, Science Park, No.2 Yikuang Street,
Harbin 150080, Heilongjiang, People's Republic of China
e-mail: wuzheperson@126.com

immersed in 40% hydrofluoric acid to remove the surface oxide film, and then they were cleaned by ultrasonic in acetone. The prepared tungsten fibers were put straightly into the clean quartz tube, and the master alloy was set above the tungsten fibers, then the composites were fabricated by means of penetrating casting method. The composites were fabricated by two kinds of heating processes, which were different at heating time at 1250 °C. In the first heating process, $W_f/Cu_{82}Al_{10}Fe_4Ni_4(30)$ composites was fabricated at 1250 °C with 30 min. In the second heating process, $W_f/Cu_{82}Al_{10}Fe_4Ni_4(60)$ composites was fabricated at 1250 °C with 60 min. Tungsten fibers volume fraction of the two kinds of composites is 80%. Three-point bending samples with the dimension of 5 mm × 5 mm × 35 mm were made by wire cutting machine. The size of impacting samples is Φ4 mm × 4 mm. Dynamic compression test was finished by split Hopkinson pressure bar (SHPB) at the strain rate of 2000 s⁻¹. To ensure the reliability of test data, each group test would be done at least three times. Then microstructure and fracture mechanism of the composites were analyzed by transmission electron microscope (TEM) and scanning electron microscope (SEM).

Results and discussion

Microstructure observation

Figure 1a is SEM image at interface in $W_f/Cu_{82}Al_{10}Fe_4Ni_4(30)$ composites, and there are interfacial reaction products on the surface of tungsten fiber. Energy Disperse Spectroscopy (EDS) insert showed tungsten, iron, nickel were the major elements of interfacial reaction products. Figure 1b was TEM image at interface in $W_f/Cu_{82}Al_{10}Fe_4Ni_4(30)$ composites, and the selected area electron diffraction pattern (SADP) insert indicated that interfacial reaction products were Fe–Ni solid solutions. The result indicated that tungsten diffuse into Fe–Ni solid solutions, which were favorable to improve wettability and interface strength between matrix and tungsten fibers in $W_f/Cu_{82}Al_{10}Fe_4Ni_4(30)$ composites. While the edge of tungsten fibers in $W_f/Cu_{82}Al_{10}Fe_4Ni_4(60)$ composites was destroyed as showed in Fig. 1c. Some long strip of grains formed at the edge of tungsten fibers in Fig. 1d, SADP insert indicated that they were tungsten grains generated by recrystallization. The result indicated that heating time

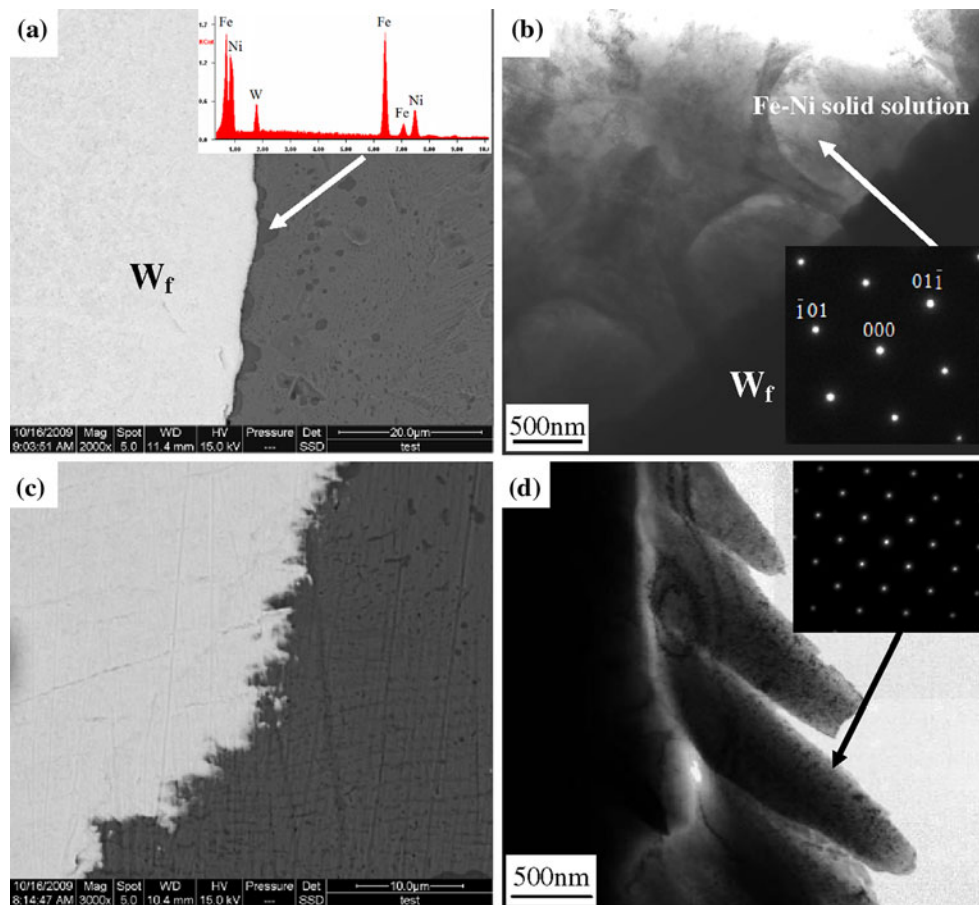


Fig. 1 The interface microstructure of the composites. **a** SEM image of $W_f/Cu_{82}Al_{10}Fe_4Ni_4(30)$ composites, **b** TEM image of $W_f/Cu_{82}Al_{10}Fe_4Ni_4(30)$ composites, **c** SEM image of $W_f/Cu_{82}Al_{10}Fe_4Ni_4(60)$ composites, **d** TEM image of $W_f/Cu_{82}Al_{10}Fe_4Ni_4(60)$ composites

had important effect on interface microstructure of the composites.

Effect of heating process on interface strength

Figure 2 is bending stress–displacement curves of $W_f/Cu_{82}Al_{10}Fe_4Ni_4(30)$ composites and $W_f/Cu_{82}Al_{10}Fe_4Ni_4(60)$ composites, from which it can be found that bending strength of $W_f/Cu_{82}Al_{10}Fe_4Ni_4(30)$ composites is obviously higher than $W_f/Cu_{82}Al_{10}Fe_4Ni_4(60)$ composites. Figure 3a and b showed fracture morphologies of $W_f/Cu_{82}Al_{10}Fe_4Ni_4(30)$ composites and $W_f/Cu_{82}Al_{10}Fe_4Ni_4(60)$ composites after three-point bending test, respectively. The damage mainly emerged within tungsten fibers in $W_f/Cu_{82}Al_{10}Fe_4Ni_4(30)$ composites in Fig. 3a, which proved that the composites possessed high interface strength. While the damage mainly occurred at the edge of tungsten fibers in $W_f/Cu_{82}Al_{10}Fe_4Ni_4(60)$ composites in Fig. 3b.

The change of interface microstructure was the main reason why fracture morphologies of $W_f/Cu_{82}Al_{10}Fe_4Ni_4(30)$ composites and $W_f/Cu_{82}Al_{10}Fe_4Ni_4(60)$ composites

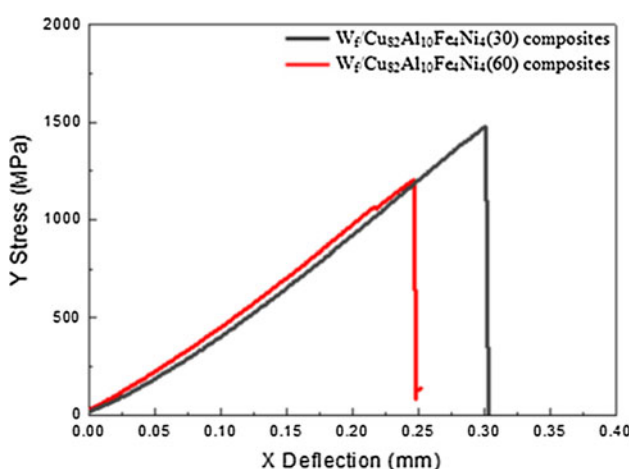
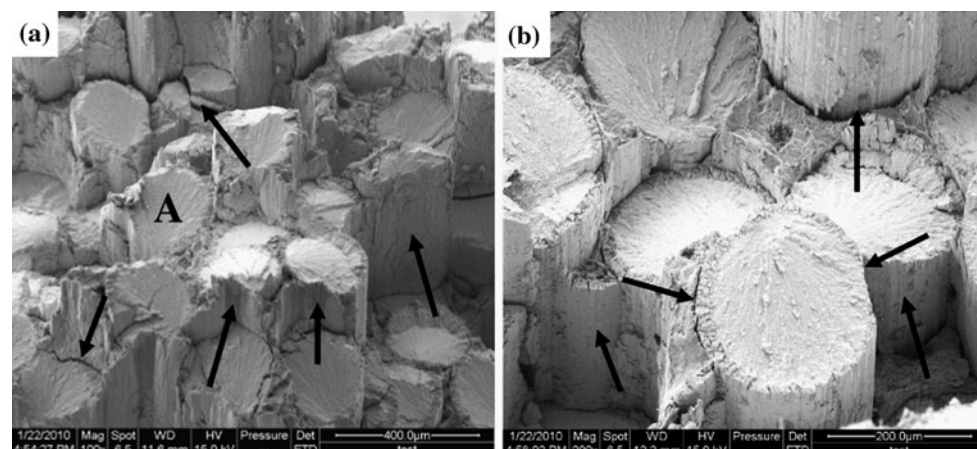


Fig. 2 Bending stress–displacement curves of the composites

Fig. 3 SEM images of three-point bending fracture surfaces of the composites. **a** $W_f/Cu_{82}Al_{10}Fe_4Ni_4(30)$ composites, **b** $W_f/Cu_{82}Al_{10}Fe_4Ni_4(60)$ composites



were different. In $W_f/Cu_{82}Al_{10}Fe_4Ni_4(30)$ composites, tungsten diffused into Fe–Ni solid solutions precipitated on the surface of tungsten fibers as showed in Fig. 1b, which improved interface strength between tungsten fibers and matrix. While there did not exist the diffusion in $W_f/Cu_{82}Al_{10}Fe_4Ni_4(60)$ composites as showed in Fig. 1d, and the recrystallization of tungsten fibers would also reduce strength of the edge of tungsten fibers, which made bending strength of $W_f/Cu_{82}Al_{10}Fe_4Ni_4(60)$ composites obviously reduce.

Fracture behaviors of the composites after dynamic compression

Figure 4 is compressive stress–strain curves of the two kinds of composites at strain rate 2000 s^{-1} . Dynamic compressive strength of $W_f/Cu_{82}Al_{10}Fe_4Ni_4(30)$ composites was 2500 Mpa, which was higher than that of $W_f/Cu_{82}Al_{10}Fe_4Ni_4(60)$ composites. The plastic strain of $W_f/Cu_{82}Al_{10}Fe_4Ni_4(30)$ composites was 0.22, while the strain of $W_f/Cu_{82}Al_{10}Fe_4Ni_4(60)$ composites at failure was only 0.09.

Figure 5a and b showed microstructure morphology of $W_f/Cu_{82}Al_{10}Fe_4Ni_4(30)$ composites after dynamic compression. Obvious plastic deformation and some cracks emerged, but overall failure did not occur in $W_f/Cu_{82}Al_{10}Fe_4Ni_4(30)$ composites as show in Fig. 5a, and the partial enlarged drawing showed there existed lots of lacerated fibrous substances in the cracks. Because the inner structure of original tungsten fiber is fibrous, the microstructure observation indicated that the cracks emerged within tungsten fibers and heating process of $W_f/Cu_{82}Al_{10}Fe_4Ni_4(30)$ composites had little effect on the inner structure of tungsten fibers. The $W_f/Cu_{82}Al_{10}Fe_4Ni_4(30)$ composites was cut along the central axis by wire cutting machine, as show in Fig. 5b, the splits mainly appeared within tungsten fiber and there existed a lot of lacerated fibrous structure, which also indicated that microstructure

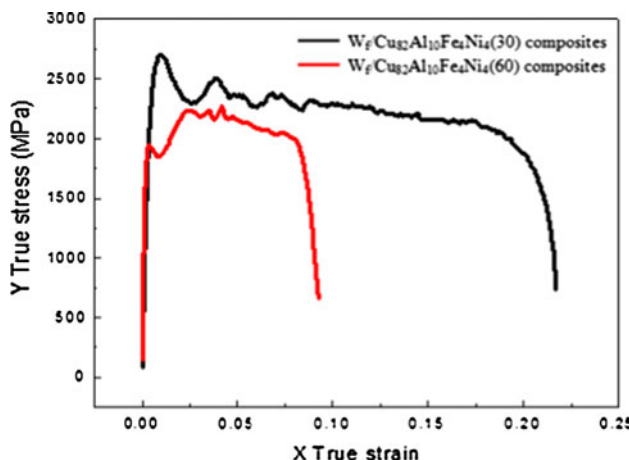


Fig. 4 Compressive stress–strain curves of the composites at the strain rate of 2000 s^{-1}

of tungsten fibers did not change and interface strength was high in the composites.

Brittle fracture occurred in $\text{W}_f/\text{Cu}_{82}\text{Al}_{10}\text{Fe}_4\text{Ni}_4(60)$ composites after dynamic compression, as showed in Fig. 5c, $\text{W}_f/\text{Cu}_{82}\text{Al}_{10}\text{Fe}_4\text{Ni}_4(60)$ composites split into two parts, and the splitting surface was smooth, on which fibrous substances within tungsten fibers were few and very coarse.

The $\text{W}_f/\text{Cu}_{82}\text{Al}_{10}\text{Fe}_4\text{Ni}_4(60)$ composites was cut along the central axis by wire cutting machine, as show in Fig. 5d, the damage appeared at the edge of tungsten fibers, indicating that strength of the edge of tungsten fibers was lowest in $\text{W}_f/\text{Cu}_{82}\text{Al}_{10}\text{Fe}_4\text{Ni}_4(60)$ composites. Any tiny fibrous substances within tungsten fibers did not been found except few coarse fibrous substances in Fig. 5c and d, which indicated that prolonged heating time made fibrous structure within tungsten fibers coarsen and even disappear in $\text{W}_f/\text{Cu}_{82}\text{Al}_{10}\text{Fe}_4\text{Ni}_4(60)$ composites. Tungsten fibers possessed high mechanical property due to the fibrous structure, while coarsening and disappearance of the fibrous structure would lead to the reduction of mechanical property of $\text{W}_f/\text{Cu}_{82}\text{Al}_{10}\text{Fe}_4\text{Ni}_4(60)$ composites.

Figure 6a, b and c were TEM microstructure of $\text{W}_f/\text{Cu}_{82}\text{Al}_{10}\text{Fe}_4\text{Ni}_4(30)$ composites and $\text{W}_f/\text{Cu}_{82}\text{Al}_{10}\text{Fe}_4\text{Ni}_4(60)$ composites after dynamic compression. The radial observation location was 1.5 mm away from the edge of the samples, and the axial observation location was middle of the samples. Figure 6a and b showed dislocation density in $\text{W}_f/\text{Cu}_{82}\text{Al}_{10}\text{Fe}_4\text{Ni}_4(60)$ composites lower than that in $\text{W}_f/\text{Cu}_{82}\text{Al}_{10}\text{Fe}_4\text{Ni}_4(30)$ composites. Due to long time heating to $\text{W}_f/\text{Cu}_{82}\text{Al}_{10}\text{Fe}_4\text{Ni}_4(60)$ composites, the strength and plasticity of tungsten fibers reduced rapidly, so brittle

Fig. 5 SEM images of the composites after dynamic compression. **a, b** $\text{W}_f/\text{Cu}_{82}\text{Al}_{10}\text{Fe}_4\text{Ni}_4(30)$ composites; **c, d** $\text{W}_f/\text{Cu}_{82}\text{Al}_{10}\text{Fe}_4\text{Ni}_4(60)$ composites

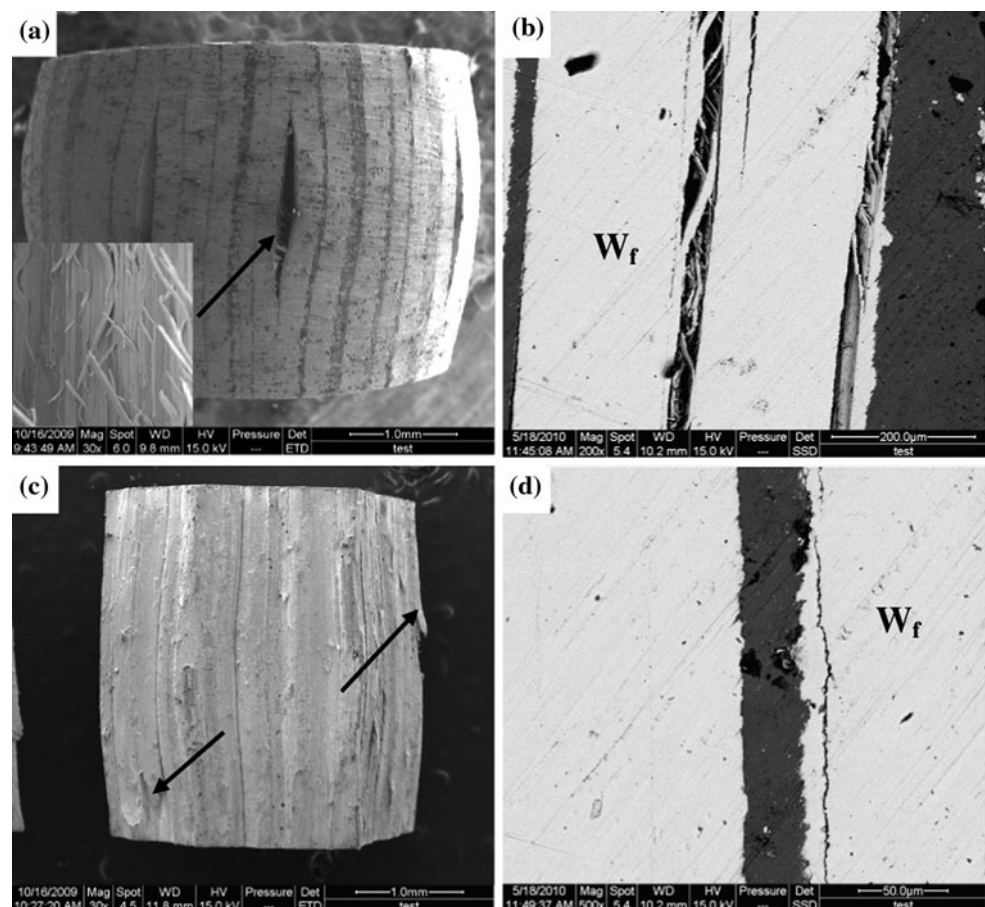
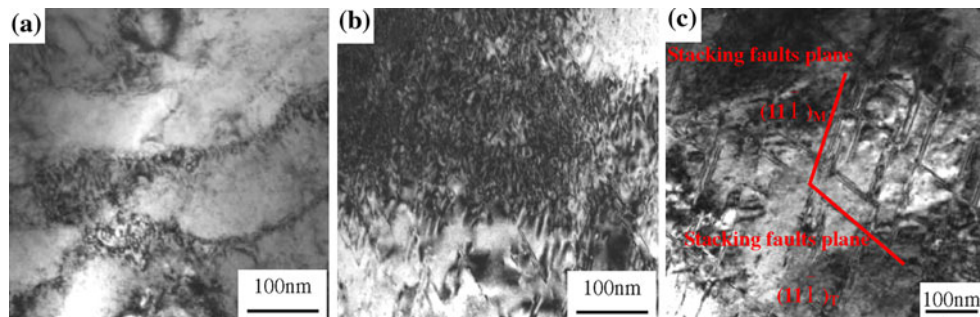


Fig. 6 TEM images of the composites after dynamic compression. **a** Dislocations in $W_f/Cu_{82}Al_{10}Fe_4Ni_4(60)$ composites, **b** dislocations in $W_f/Cu_{82}Al_{10}Fe_4Ni_4(30)$ composites, **c** stacking faults in $W_f/Cu_{82}Al_{10}Fe_4Ni_4(30)$ composites



fracture occurred in tungsten fibers easily when the composites was impacted. This meant that deformation of $W_f/Cu_{82}Al_{10}Fe_4Ni_4(60)$ composites was very little when overall failure happen, so the dislocation density in matrix was relatively low as showed in Fig. 6a. While tungsten fibers in $W_f/Cu_{82}Al_{10}Fe_4Ni_4(30)$ composites possessed excellent plasticity, and $W_f/Cu_{82}Al_{10}Fe_4Ni_4(30)$ composites also possessed high interface strength. The load could be transferred smoothly between matrix and tungsten fibers when $W_f/Cu_{82}Al_{10}Fe_4Ni_4(30)$ composites was impacted, which only caused obvious plastic deformation and avoided overall failure of the composites, so the dislocation density in the matrix also increase significantly as showed in Fig. 6b. It was also found that there were stacking faults of two directions crossing one another inside a grain in matrix of $W_f/Cu_{82}Al_{10}Fe_4Ni_4(30)$ composites in Fig. 6c. If the direction of the external force was parallel to the $[2\bar{1}\bar{1}]$ crystalline direction of this grain, the atoms on a $(11\bar{1})$ plane would slip with a distance of $[2\bar{1}\bar{1}]/6$ along $[2\bar{1}\bar{1}]$ direction and the atoms of next $(11\bar{1})$ plane would slip with the same distance, which resulted in the change of stacking sequence and then formation of a slice of stacking fault. As the atoms on any $(11\bar{1})$ plane under the action of external force along $[2\bar{1}\bar{1}]$ direction might have the chance to slip, at the moment under the action of external force, there would be several slices of stacking faults to be formed. As continuing deformation, the orientation of this grain changed. When the direction of the external force was the $[211]$ direction, the atoms on a $(11\bar{1})$ plane would slip with a distance of $[211]/6$ along $[211]$ direction, and then the stacking faults formed. So there would be stacking faults of two directions crossing one another inside a grain.

Conclusions

The interface microstructure of $W_f/Cu_{82}Al_{10}Fe_4Ni_4(30)$ composites and $W_f/Cu_{82}Al_{10}Fe_4Ni_4(60)$ composites were different. A little of tungsten diffused into the Fe–Ni solid solutions precipitated on the surface of tungsten fibers in $W_f/Cu_{82}Al_{10}Fe_4Ni_4(30)$ composites, which would improve

interface strength of the composites. While long strip of tungsten grains generated by recrystallization occurred at the edge of tungsten fibers in $W_f/Cu_{82}Al_{10}Fe_4Ni_4(60)$ composites, which would reduce the strength of the composites. Dynamic compression test indicated that $W_f/Cu_{82}Al_{10}Fe_4Ni_4(30)$ composites possessed higher strength and plasticity than $W_f/Cu_{82}Al_{10}Fe_4Ni_4(60)$ composites. Inner structure of tungsten fibers in $W_f/Cu_{82}Al_{10}Fe_4Ni_4(60)$ composites was consistent with that of original tungsten fibers, which indicated that heating process of $W_f/Cu_{82}Al_{10}Fe_4Ni_4(30)$ composites had little effect on the inner structure of tungsten fibers. While tiny fibrous structure within tungsten fibers coarsened and even disappeared in $W_f/Cu_{82}Al_{10}Fe_4Ni_4(60)$ composites, which indicated that the extension of heating time would change the inner structure of tungsten fibers.

References

- Pappu S, Kennedy C, Murr LE, Magness LS, Kapoor D (1999) Mater Sci Eng A 262:115
- Lair S, Randrianarivony FM, Quinones SA, Murr LE (2002) J Mater Sci 37:5197. doi:[10.1023/A:1021083800238](https://doi.org/10.1023/A:1021083800238)
- Liu JX, Li SK, Fan AL, Sun HC (2008) Mater Sci Eng A 487:235
- Conner RD, Dandliker RB, Johnson WL (1998) Acta Mater 46:6089
- Zhang HF, Li H, Wang AM, Fu HM, Ding BZ, Hu ZQ (2009) Intermetallics 17:1070
- Kim HG, Kim KT (2000) Int J Mech Sci 42:1339
- Manel RR, Jan O (2009) Eng Fract Mech 76:1485
- Schade P (2000) Int J Refract Metals Hard Mater 28:648
- Schade P (2006) Int J Refract Metals Hard Mater 24:332
- Ma WF, Kou HC, Chen CS, Li JS, Chang H, Zhou L, Fu HZ (2008) Mater Sci Eng A 486:308
- Qiu KQ, Wang AM, Zhang HF, Ding BZ, Hua ZQ (2002) Intermetallics 10:1283
- Jedamzik R, Neubrand A, Rödel J (2000) J Mater Sci 35:477. doi:[10.1023/A:1004735904984](https://doi.org/10.1023/A:1004735904984)
- Cheng JG, Wan L, Cai YB, Zhu JC, Song P, Dong J (2010) J Mater Process Technol 1:137
- Hong SH, Kim BK, Munir ZA (2005) Mater Sci Eng A 405:325
- Ibrahim A, Abdallah M, Mostafa SF, Hegazy AA (2009) Mater Des 30:1398
- Doré Lay S, Eustathopoulos N, Allibert CH (2003) Scr Mater 49:237